How temporal patterns in rainfall determine the geomorphology and carbon fluxes of tropical peatlands

How temporal patterns in rainfall determine the geomorphology and carbon fluxes of tropical peatlands

Alexander R. Cobb[a,1], Alison M. Hoyt[b], Laure Gandois[c], Jangarun Eri[d], René Dommain[e,f], Kamariah Abu Salim[g], Fuu Ming Kai[a,2], Nur Salihah Haji Su'ut[h], and Charles F. Harvey[a,b]

[a]Center for Environmental Sensing and Modeling, Singapore–MIT Alliance for Research and Technology, 138602 Singapore; [b]Department of Civil and Environmental Engineering, Massachusetts Institute of Technology, Cambridge, MA 02139; [c]Laboratoire Écologie Fonctionnelle et Environnement, Université de Toulouse, CNRS, Institut National Polytechnique de Toulouse, Université Paul Sabatier, F-31326 Castanet-Tolosan, France; [d]Forestry Department, Ministry of Industry and Primary Resources, Jalan Menteri Besar, Bandar Seri Begawan BB3910, Brunei Darussalam; [e]Department of Anthropology, Smithsonian Institution, National Museum of Natural History, Washington, DC 20560; [f]Institute of Earth and Environmental Science, University of Potsdam, 14476 Potsdam, Germany; [g]Biology Programme, Universiti Brunei Darussalam, Bandar Seri Begawan BE1410, Brunei Darussalam; and [h]Brunei Darussalam Heart of Borneo Centre, Ministry of Industry and Primary Resources, Jalan Menteri Besar, Bandar Seri Begawan BB3910, Brunei Darussalam

Edited by Donald E. Canfield, Institute of Biology and Nordic Center for Earth Evolution, University of Southern Denmark, Odense M., Denmark, and approved May 5, 2017 (received for review February 6, 2017)

Tropical peatlands now emit hundreds of megatons of carbon dioxide per year because of human disruption of the feedbacks that link peat accumulation and groundwater hydrology. However, no quantitative theory has existed for how patterns of carbon storage and release accompanying growth and subsidence of tropical peatlands are affected by climate and disturbance. Using comprehensive data from a pristine peatland in Brunei Darussalam, we show how rainfall and groundwater flow determine a shape parameter (the Laplacian of the peat surface elevation) that specifies, under a given rainfall regime, the ultimate, stable morphology, and hence carbon storage, of a tropical peatland within a network of rivers or canals. We find that peatlands reach their ultimate shape first at the edges of peat domes where they are bounded by rivers, so that the rate of carbon uptake accompanying their growth is proportional to the area of the still-growing dome interior. We use this model to study how tropical peatland carbon storage and fluxes are controlled by changes in climate, sea level, and drainage networks. We find that fluctuations in net precipitation on timescales from hours to years can reduce long-term peat accumulation. Our mathematical and numerical models can be used to predict long-term effects of changes in temporal rainfall patterns and drainage networks on tropical peatland geomorphology and carbon storage.

tropical peatlands | peatland geomorphology | peatland hydrology | peatland carbon storage | climate-carbon cycle feedbacks

Tropical peatlands store gigatons of carbon in peat domes, gently mounded land forms kilometers across and 10 or more meters high (1). The carbon stored as peat in these domes has been sequestered by photosynthesis of peat swamp trees (2) and preserved for thousands of years by waterlogging, which suppresses decomposition. Human disturbance of tropical peatlands by fire and drainage for agriculture is now causing reemission of that carbon at rates of hundreds of megatons per year (2–5): Emissions from Southeast Asian peatlands alone are equivalent to about 2% of global fossil fuel emissions or 20% of global land use and land cover change emissions (6, 7). Because peat is mostly organic carbon, a description of the growth and subsidence of tropical peatlands also quantifies fluxes of carbon dioxide (1, 4, 8). Evidence from a range of studies establishes that accumulation and loss of tropical peat are controlled by water table dynamics (4, 9). When the water table is low, aerobic decomposition occurs, releasing carbon dioxide; when the water table is high, aerobic decomposition is inhibited by lack of oxygen, production of peat exceeds its decay, and peat accumulates. In this way, the rate of peat accumulation is determined by the fraction of time that peat is exposed by a low water table (Fig. 1).

The water table rises and falls in a peatland according to the balance between rainfall, evapotranspiration, and groundwater flow. Water flows downslope toward the edge of each peat dome, where it is bounded by rivers. This flow occurs at a rate limited by the hydraulic transmissivity of the peat—the efficiency with which it conducts lateral flow—and follows the gradient in the water table. The gradient in the water table is slightly steeper near dome boundaries where the flow of water is faster. A steeper gradient near boundaries implies a domed shape in the water table, or groundwater mound, corresponding to the domed shape of the peat surface. The doming of the peat surface is very subtle: Gradients are about 1 m/km (1). Nonetheless, it is the dome's gentle curvature that accounts for the carbon storage within the drainage boundary.

Significance

A dataset from one of the last protected tropical peat swamps in Southeast Asia reveals how fluctuations in rainfall on yearly and shorter timescales affect the growth and subsidence of tropical peatlands over thousands of years. The pattern of rainfall and the permeability of the peat together determine a particular curvature of the peat surface that defines the amount of naturally sequestered carbon stored in the peatland over time. This principle can be used to calculate the long-term carbon dioxide emissions driven by changes in climate and tropical peatland drainage. The results suggest that greater seasonality projected by climate models could lead to carbon dioxide emissions, instead of sequestration, from otherwise undisturbed peat swamps.

Author contributions: A.R.C. and C.F.H. designed research; A.R.C. and J.E. established the field site; A.R.C., A.M.H., L.G., J.E., R.D., K.A.S., F.M.K., and N.S.H.S. performed research; A.R.C. contributed new analytic tools; A.R.C., A.M.H., and C.F.H. analyzed data; and A.R.C. and C.F.H. wrote the paper.

The authors declare no conflict of interest.

This article is a PNAS Direct Submission.

Freely available online through the PNAS open access option.

Data deposition: The data reported in this paper have been deposited in the Dryad Digital Repository (dx.doi.org/10.5061/dryad.18q5n).

[1]To whom correspondence should be addressed. Email: alex.cobb@smart.mit.edu.

[2]Present address: Gas Metrology Laboratory, National Metrology Center, Agency for Science, Technology and Research, 118221 Singapore.

This article contains supporting information online at www.pnas.org/lookup/suppl/doi:10.1073/pnas.1701090114/-/DCSupplemental.

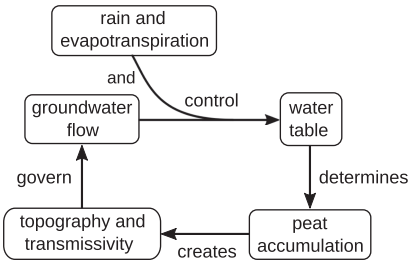

Fig. 1. Ecosystem feedback leading to peat accumulation. Peat accumulation occurs because of waterlogging of plant remains and is therefore determined by the proportion of time that peat is protected from aerobic decomposition by a high water table. Over time, peat builds up into gently mounded land forms, or domes, bounded by rivers. The slopes in a peat dome, although very small, govern groundwater flow toward bounding rivers at rates limited by the transmissivity of the peat.

Once the peatland surface is sufficiently domed, water is shed so rapidly that no more organic matter can be waterlogged within the confines of the drainage network, and peat accumulation stops (10). This maximally domed shape sets a limit on how much carbon a peat dome can sequester and preserve under a given rainfall regime (11). If the peat dome is flatter than its stable shape for the current climate, it will sequester carbon and grow; if it is more domed than its stable shape, it will release carbon and subside as peat decomposes. [In the tropical peat literature, "subsidence" is used for a decline in the peat surface elevation, regardless of mechanism (5).] The volume of this stable shape times the average carbon density of the peat defines a capacity for storage of carbon as peat within the drainage boundary.

If we can predict the stable shapes of peat domes and how they evolve over time in a given climate, we can determine how peatland carbon storage capacity and carbon fluxes are affected by changes in rainfall regime, drainage network, and sea level. However, when predicting the stable shapes of peat domes and their evolution toward these shapes, there are two complicating factors: (*i*) The boundaries imposed by drainage networks have complex shapes and (*ii*) rainfall is intermittent and variable. The water table rises during rainstorms and falls during dry periods, even when the peat surface is stable. These fluctuations in the water table seem to be important because it is widely believed that seasonality of rainfall affects tropical peat accumulation (12, 13). But how should we take these fluctuations into account to predict the slow development and stable shapes of peat domes? Understanding the global impact of changes in rainfall amount and variability, drainage networks, and sea level on tropical peatland carbon storage and fluxes requires a theory that can accommodate the complicated drainage networks and intermittent rainfall of the real world.

Ingram (10) made the first prediction of the limiting shape of a temperate peat dome imposed by the balance between rainfall and groundwater flow. Assuming constant rainfall, he computed the steady-state shape of a peat dome with uniform permeability between parallel rivers. Clymo (14) later developed a simple dynamic model for accumulation of peat at a single point in the landscape. Clymo's model assumed that the thickness of peat above the water table would not change and focused on anaerobic decomposition in deeper waterlogged peat. Hilbert et al. (15) later built on Clymo's model to allow a varying thickness of peat above the water table via a simple water balance whereby drainage increases linearly with peat surface elevation. Hilbert's model inspired a series of increasingly sophisticated models for vegetation dynamics and peat accumulation at a point. The most recent of these point models computes water table depth from monthly rainfall, using a site-specific model (16). Meanwhile, numerical models have been used to simulate peat accumulation under constant rainfall (17, 18). Although these subsequent works simulate the dynamics of peat production and decomposition in increasing detail, a strength of Ingram's model was that it provided quantitative intuition for how peat dome morphology depends on peat hydrologic properties and average rainfall. Could a principle like Ingram's exist that describes peatland dynamics as well as statics and remains applicable with realistic drainage networks and rainfall regimes?

We established a field site in one of the last pristine peat swamp forests in Southeast Asia and then used measurements from this site to develop a mathematical model for the geomorphic evolution of tropical peatlands that is simpler, yet more general than Ingram's model for high-latitude peatlands. Our model makes it possible to predict effects of changes in rainfall regime and drainage networks on carbon storage and fluxes in tropical peatlands. The model predicted, perhaps surprisingly, that surface peat would be older near dome margins. We tested these predictions by radiocarbon dating core samples and comparing the age of each sample to the simulated age at its location and depth. Finally, we explored the future of tropical peatlands under climate projections by simulating the geomorphic evolution of an idealized peat dome under projected changes in rainfall patterns and drainage.

Methods

Field Measurements. We established a field site in a pristine peat forest in Brunei Darussalam (Borneo) to study a peat dome where current processes affecting peat accumulation are essentially similar to those during its long-term development (Fig. 2). At the site, we installed 5 piezometers along a 2.5-km trail, 12 piezometers along a 180-m transect, and 3 throughfall gauges. We completed a total station survey of peat surface elevation along the transect to characterize peat surface microtopography. To characterize large-scale peatland morphology, we also obtained LiDAR data for the entire study area. To study peat dome development, we collected nine peat cores from which we obtained 35 radiocarbon dates. To test whether our undisturbed site behaved similarly to sites studied by other groups, we installed four soil respiration chambers and a piezometer at a nearby logged but undrained site.

Morphology vs. Microtopography. Superimposed on the gross morphology of a peat dome is a fine microtopography of meter-scale depressions, or hollows, separated by higher areas, or hummocks (19, 20). The hummocks consist of partly decomposed logs, branches, and leaves lodged among living buttresses, stilt roots, pneumatophores, and giant rhizomes. Whereas the microtopography in high-latitude peat bogs may have regular and oriented patterns (21), surveys by Lampela et al. (20) in a tropical peat swamp in Central Kalimantan showed no orientation or regularity. Similarly, our microtopography survey and other observations revealed no regular patterns or channels in peat dome microtopography.

In describing the evolution of peat dome morphology, we want to capture the effects of the hummock-and-hollow microtopography without explicitly simulating its details. Measurements from the 12 piezometers along our microtopography transect showed that the water table is relatively smooth, even though the peat surface is highly irregular on a spatial scale of centimeters to meters (Fig. 3). We therefore represent the peat surface by a reference surface p, smooth like the water table, that underlies the actual peat surface $\tilde{p}$. We refer to this reference surface p as the land surface. The peat surface $\tilde{p}$ is a "texture" that sits on the smooth land surface p. The bottoms of hollows provide the most readily identifiable local reference elevation (20), so we define the land surface p as a smooth surface fit through the bottoms of hollows (local minima in the peat surface $\tilde{p}$). On the basis of this definition, we determined the current land surface at our site by smoothing a raster map obtained from local minima in LiDAR last-return points. We also used the transect survey and piezometer data to find the land surface p along the microtopography survey transect (*SI Methods*).

Groundwater Flow. We model the dynamics of the water table H subject to net precipitation q_n (rainfall intensity R minus evapotranspiration, ET), using Boussinesq's equation for essentially horizontal groundwater flow

$$S_y \frac{\partial H}{\partial t} = q_n + \nabla \cdot (T \nabla H), \quad [1]$$

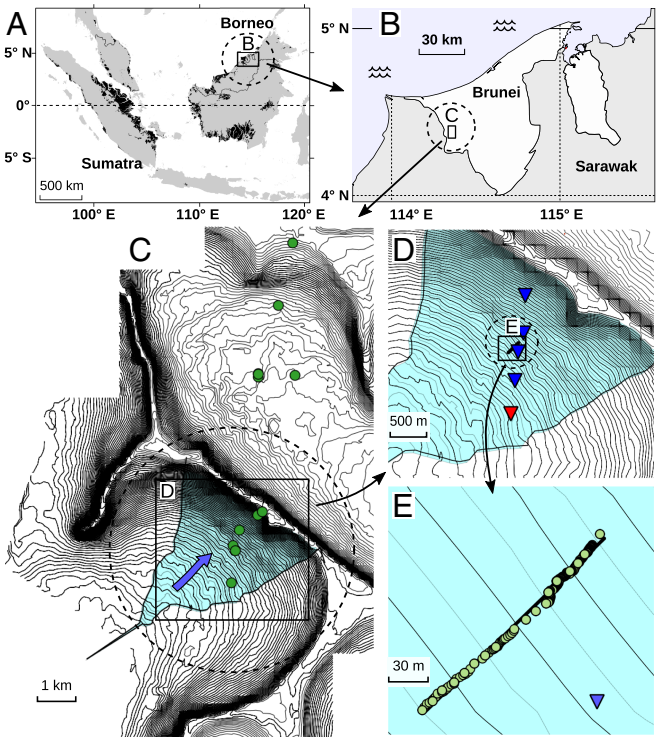

Fig. 2. Site of field data collection in Brunei Darussalam. (*A*) Distribution of peatlands in Borneo, Sumatra, and Peninsular Malaysia. (*B*) Field site in Brunei Darussalam, on Borneo island. (*C*) Contour map of study area from airborne LiDAR data, showing radiocarbon-dated peat cores (green points) at a primary site (Mendaram, south) and a degraded site (Damit, north) and the boundaries of the flow tube used for hydrologic simulations (blue). (*D*) Piezometers (triangles) at the Mendaram site (colors are explained in Fig. 6). (*E*) Survey points in microtopography transect (Fig. 3*B*).

where the specific yield S_y is the amount of water required for a differential increment in water table elevation, and transmissivity T is the volumetric flow per perimeter driven by a particular head gradient ∇H. Boussinesq's equation is a standard groundwater modeling equation for flow domains like peatlands that are much wider than they are thick.

At high water tables, hollows become flooded from saturation of the peat below, forming small pools. These pools are not connected into channels (20) and therefore do not allow open-channel flow on a large scale in the peatland. Instead, flow through the peatland is limited by flow through the porous matrix of the hummocks between these isolated pools. We apply Boussinesq's equation at scales much larger than hummocks and hollows (tens of meters) and refer to the flow of water through the peatland as "groundwater flow" even though some flow occurs above the local peat surface, in hollows, during wet periods. Boussinesq's equation requires only that lateral flow is proportional to the head gradient, which is the case if the overall flow is limited by laminar flow through hummocks. We never observed ephemeral channels connecting hollows within the peatland in our 6 y at the site. In addition, if flow were nonlaminar, we would expect different local flow behavior at the same water table height in areas with different water table gradients, but instead water table behavior is uniform (*Results and Discussion*).

Local Carbon Balance. A broad range of studies demonstrates that the thickness of peat exposed above the water table determines the rate of peat accumulation or loss (4, 22). Like others (4, 22), we modeled the dynamics of peat accumulation or loss $\partial p/\partial t$ as the difference between the rate of peat production f_p when the water table is at the land surface and the rate of peat loss by decomposition $(p - H)\alpha$, which is the thickness $p - H$ of peat exposed above the water table times a decomposition rate constant α,

$$\frac{\partial p}{\partial t} = f_p - (p - H)\alpha \qquad [2]$$

(Fig. 4). The peat surface is stable, neither growing nor subsiding $\langle \partial p/\partial t \rangle = 0$ wherever the water table fluctuates in such a way that peat production is balanced by decomposition over time

$$f_p = \langle p - H \rangle \alpha, \qquad [3]$$

where angle brackets $\langle \cdot \rangle$ indicate a time average.

Several other studies have shown a leveling off of soil CO_2 efflux at very low water tables (25, 26), and it is also likely that very high water tables ultimately limit net carbon uptake by trees (primary production) (16). However, including these effects did not affect simulations because these extreme water table heights and depths were neither observed at our site nor predicted by simulations of our site. We also did not include anaerobic decomposition below the water table because analyses of peat cores from tropical sites in Asia (2), including our site (27), do not show detectable loss of waterlogged peat from anaerobic decomposition.

Numerical Simulations. We built a numerical model of waterlogging and peat accumulation based on Eqs. **1** and **2** to simulate peat dome geomorphogenesis and carbon fluxes. These two equations are coupled by the water table elevation H and the peat surface elevation p, both of which vary in time and space. The equations require four parameters: (*i*) a specific yield function S_y, (*ii*) a transmissivity function T, (*iii*) a rate of peat production f_p, and (*iv*) a decomposition rate constant α. The model uses a finite volume scheme (Fig. S1) with special features designed to handle the severe nonlinearity of the transmissivity function T (*SI Expanded Description of Peat Dome Simulation*).

We determined the specific yield and transmissivity functions S_y, T from the response of the water table to heavy rain and dry spells (*Results and Discussion*). We then fitted the parameters for peat accumulation f_p, α by simulating the 2,700-y evolution of a peat dome at our field site in Brunei and matching the simulated modern peat surface to the peat surface measured by LiDAR. We tested our model against radiocarbon dates from peat cores extracted from the peatland and then used the model to answer general questions about carbon fluxes from tropical peatlands after perturbation by climate change and drainage.

Limitations of Modeling Approach. Our goal was to build the simplest model that can make reasonable quantitative predictions of tropical peat dome dynamics. In most Southeast Asian peatland complexes, every area between rivers is occupied by a peat dome, so it is not apparent how any peat dome could now expand to fill a larger area. However, domes tend to be larger in older peatlands, suggesting a long-term process of dome coalescence. We did not attempt to model these long-term changes in river networks. We also did not consider changes in hydraulic conductivity near the surface caused by compaction or changes in microtopography under agriculture.

Results and Discussion

Carbon Storage Capacity of Tropical Peatlands.

Local water balance is dominated by flows near the surface. Eighteen months of data on water table height in five piezometers along a 2.5-km transect (Fig. 5) show two distinctive features of water table behavior in tropical peatlands. First, when the water table is high, it falls very rapidly; and second, the water table height relative to the land surface remains approximately uniform in all piezometers as the water table rises and falls, as observed elsewhere by Hooijer (28). In what follows, we use "water table height" $\zeta = H - p$ to refer to the water table height relative to the land surface, as distinct from the water table elevation H above mean sea level. Because the water table height ζ is approximately uniform, the water table behavior can be summarized by a pair of curves describing the uniform rise of the water table during heavy rain and the uniform decline of the water table during dry intervals between rains (Fig. 5 *E* and *F*). During heavy rain, the effects of evapotranspiration and outward flow are negligible, and the rainfall intensity vs. rate of increase in water table height gives the specific yield. Between rain events, the water table declines because of evapotranspiration and the divergence of groundwater flow.

Transmissivity T is a function of water table height ζ and controls the divergence of groundwater flow $\nabla \cdot (T \nabla H)$. We determined the effect of water table height on transmissivity

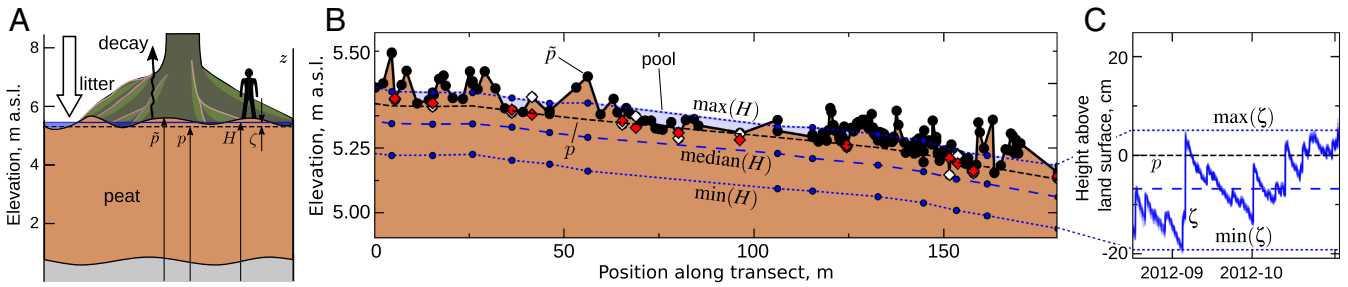

Fig. 3. Microtopography and water table dynamics in a tropical peatland. (*A*) Cartoon of tropical peat cross-section showing variables $\tilde{p}$, the peat surface; p, the "land surface," a smooth surface fit through local minima in $\tilde{p}$; H, water table elevation; and ζ, water table height relative to the land surface, $\zeta = H - p$. The peat surface $\tilde{p}$ is irregular on a spatial scale of meters, with higher areas (hummocks) separating local depressions (hollows) that are not connected into channels. (*B*) Total station survey of peat elevation $\tilde{p}$ (black circles) along a transect and the land surface p (dashed black line). The minimum, median, and maximum water table elevations H from each of 12 piezometers along the transect are also shown (dashed blue lines). The absolute elevation of the survey points comes from matching local minima among survey points within 20-m × 20-m squares (white diamonds) with local minima in LiDAR last return data within the same squares (red diamonds). The land surface p is represented by the dashed horizontal black line. (*C*) Water table dynamics along a survey transect (*B*) in late 2012, relative to the land surface p. What appears to be a single blue line is superimposed data from the 12 piezometers shown in *B*. Also shown are the average minimum, median, and maximum water table elevations above the land surface during the same time period for all 12 piezometers.

using our water table data. The water table declines during dry intervals because of a combination of evapotranspiration and the divergence of groundwater flow; however, the two are easily distinguished at low water tables because evapotranspiration ceases at night (Fig. 5*D*). Therefore, we can obtain the divergence of groundwater flow from the declining water table during dry intervals after accounting for evapotranspiration (refs. 28, 29; further details are in *SI Methods*). We find that transmissivity increases exponentially at high water tables, when water rises into hollows and flows through hummocks, but decreases dramatically at low water tables when water flows through fine pores in the peat matrix (Fig. 5*C*). Very high permeability near the peat surface is consistent with our observations of more void space higher in the peat profile and also with recent data from other tropical peatlands (30). The water table curves (Fig. 5 *E* and *F*) indicate that the near-surface permeability is so great that the total thickness of deeper peat is unimportant for groundwater flow. Therefore, transmissivity is approximately independent of peat depth and depends only on the water table height ζ, which is uniform in space (although highly variable in time).

Morphology of peat surface explains uniform water table behavior. According to Boussinesq's equation, uniform transmissivity is not, by itself, enough to explain the uniform fluctuation of the water table. Even in hydrologic systems where hydraulic properties are uniform, the water table can behave differently at different locations because of topography. For example, in most hydrologic systems a rainstorm drives a different water table response at a topographic divide than it does near where groundwater discharges to a river.

To understand the uniform water table behavior in peatlands, we refer back to Boussinesq's equation (Eq. **1**). If both the specific yield S_y and the transmissivity T depend only on the local water table height relative to the surface and not on position within the peatland, uniform water table movement occurs if the divergence of the peat surface gradient, or the peat surface Laplacian $\nabla^2 p$, is uniform (Fig. S2 *C–E*). (The "Laplacian of the peat surface" $\nabla^2 p$, or just "Laplacian," is the scalar result of applying the Laplacian operator ∇^2 to the land surface elevation p.) To see why a uniform land surface Laplacian explains uniform water table behavior, we rewrite Boussinesq's equation (Eq. **1**) in terms of the water table height relative to the land surface ($\zeta = H - p$), instead of the water table elevation H:

$$S_y \frac{\partial (p+\zeta)}{\partial t} = q_n + \nabla \cdot [T \nabla (p+\zeta)]. \qquad [4]$$

We observe that water table height is uniform ($\nabla \zeta = \mathbf{0}$). If transmissivity T is also spatially uniform, the groundwater divergence term simplifies to the transmissivity times the peat surface Laplacian ($\nabla \cdot [T \nabla (p+\zeta)] = T \nabla^2 p$). The time derivative $\partial p / \partial t$ of the land surface elevation is negligible because peat accumulation or loss is much slower than rise or fall of the water table, so the term p can be dropped from the time derivative. We observe that the fluctuations in water table height $\partial \zeta / \partial t$ are uniform, as is net precipitation q_n, so the groundwater divergence term $T \nabla^2 p$ must also be spatially uniform. Thus, Boussinesq's equation simplifies to an ordinary differential equation (ODE) describing the uniform fluctuation of the water table relative to the peat surface

$$S_y \frac{d\zeta}{dt} = q_n + T \nabla^2 p, \qquad [5]$$

where the peat surface Laplacian $\nabla^2 p$ is uniform.

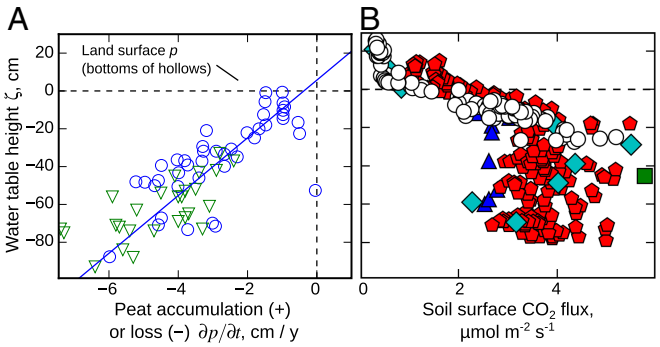

Fig. 4. Peat accumulation and CO_2 flux vs. water table height in tropical peatlands. (*A*) Peat accumulation represents the balance between peat production and decomposition. (*B*) Aerobic decomposition is one of the two main sources of peat surface CO_2 flux; the other source is root respiration. *A* shows peat accumulation or loss vs. water table height from model calibration (solid line) and from literature subsidence data (circles, ref. 4; triangles, ref. 22). The straight line was not fitted to these data, but rather arose naturally from calibration to match the modern surface of the Mendaram peat dome (Fig. 7). In *B*, soil surface CO_2 flux vs. water table height at our site in Brunei Darussalam (white circles) was very similar to fluxes in other tropical peatlands (squares, ref. 23; diamonds, ref. 19; triangles, ref. 24; pentagons, ref. 9; and hexagons, ref. 25).

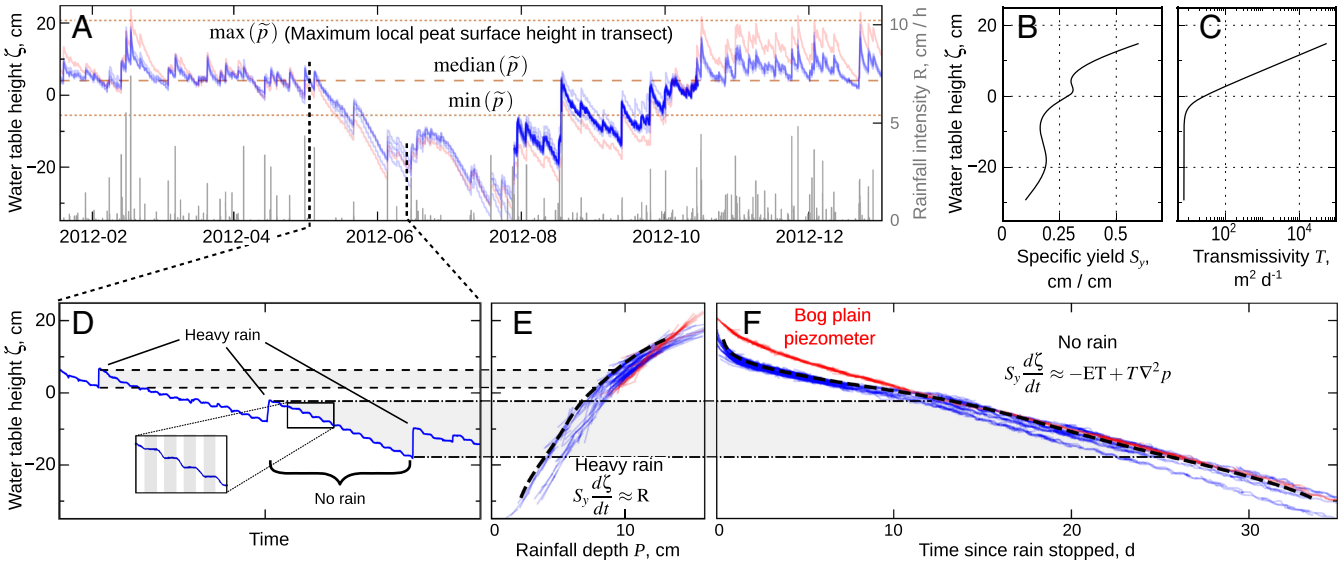

Fig. 5. Site hydrology and calibration. (*A*) Superimposed water table height (jagged blue lines) from five piezometers spanning 2.5 km and rainfall intensity (vertical lines) from three automated rain gauges over a 10-m interval. The piezometer farthest from the river (red) lies in a region with a different surface Laplacian (the "bog plain"), corresponding to an area of current peat accumulation (Fig. 6). Also shown are the minimum, median, and maximum local peat surface elevation (dashed horizontal lines) from a 180-m microtopography survey transect (Fig. 3). (*B*, *C*, *E*, and *F*) Hillslope-scale specific yield and transmissivity curves for field site (*B* and *C*), determined from recharge and recession curves (*E* and *F*). (*D*) Short interval of water table data from a single piezometer selected from *A*. *D*, *Inset* shows declining water tables during the day (unshaded) and steady water tables at night (shaded) driven by diurnal cycles of evapotranspiration. (*E* and *F*) Master recharge curve (*E*) and recession curve (*F*) assembled from intervals of heavy rain and no rain, respectively, by alignment of sequences with overlapping water table depth. During heavy rain, net precipitation intensity $q_n = R - ET$ is dominated by rainfall intensity R (*E*); with no rain, net precipitation consists only of evapotranspiration ET (*F*). Dashed black lines in *E* and *F* show water table response computed from specific yield and transmissivity (*B* and *C*), and blue translucent lines are assembled from field data in *A*. As in *A*, the red curve is from the piezometer in the flatter bog plain region (Fig. 6).

The peat surface Laplacian describes the curvature of the peat surface: It is equal to the sum of the second derivatives of the surface elevation in two perpendicular horizontal directions ($\nabla^2 p = \partial^2 p/\partial x^2 + \partial^2 p/\partial y^2$). Thus, analysis of water table dynamics predicts uniform curvature of the peat surface where water table fluctuations are uniform. This uniformity of surface elevation curvature can be tested against elevation maps.

Maps of the peat surface Laplacian are highly sensitive to microtopographic noise in the surface elevation map because the Laplacian uses the second derivative of the surface elevation. However, by the divergence theorem, the average Laplacian within any closed contour is equal to the integral of the normal gradient along the contour divided by the enclosed area. Therefore, we can examine the uniformity of the surface Laplacian by studying the slope of a regression between the integrated normal gradient and the enclosed area (Fig. 6). Indeed, we find a linear relationship between the integrated normal gradient along each contour and the area enclosed by the contour in our LiDAR-derived peat surface elevation map, indicating a uniform surface Laplacian in the region of uniform water table behavior (Fig. 6). In contrast, outside the region of uniform Laplacian, the water table behaves differently ("bog plain piezometer" in Figs. 5 and 6).

Uniform surface Laplacian determines stable tropical peatland morphology. The uniform peat surface Laplacian provides a remarkably simple way to compute a stable morphology for a tropical peat dome. By "stable morphology," we mean a morphology in which the peat surface and water table continue to fluctuate with the vagaries of climate, but there is no long-term average change in the peat surface or water table elevation (they are stationary; $\langle \partial p/\partial t \rangle = 0$, $\langle \partial H/\partial t \rangle = 0$). Uniform water table height is the simplest behavior that could make an entire peatland stable, because if the water table height is spatially uniform, the local rate of peat accumulation is also uniform. In a stable peatland, there is no long-term change in the water table height, so any water added by net precipitation must eventually be removed by groundwater flow

$$0 = \left\langle S_y \frac{d\zeta}{dt} \right\rangle = \langle q_n \rangle + \langle T \rangle \nabla^2 p_\infty. \quad [6]$$

Thus, the Laplacian $\nabla^2 p_\infty$ of the stable peatland surface p_∞ is minus the average net precipitation divided by the average transmissivity

$$\nabla^2 p_\infty = -\frac{\langle q_n \rangle}{\langle T \rangle}. \quad [7]$$

We can compute the stable topography of any tropical peatland by solving Poisson's equation (Eq. **7**) for the stable peat surface morphology p_∞, using the appropriate Laplacian value for that climate. The average transmissivity $\langle T \rangle$ is a complicated function of the temporal pattern of rainfall and the hydrologic–biological system. However, for any rainfall regime, one can find the stable surface Laplacian $\nabla^2 p_\infty$ by repeatedly simulating water table fluctuations (Eq. **5**) with a trial Laplacian $\nabla^2 p$ and adjusting the Laplacian value until peat production balances decomposition (Eq. **3**) everywhere in the peatland (*SI Methods*). In this way, one finds a shape parameter ($\nabla^2 p_\infty$) that describes stable peatland morphology under a given rainfall regime in any drainage network.

Climate and drainage network determine tropical peatland carbon storage capacity. By specifying the stable peatland topography, the uniform-Laplacian principle gives the peat carbon storage capacity inside any drainage boundary and in any given climate. The volume under the surface satisfying Poisson's equation times the mean carbon density of the peat gives the carbon storage capacity of the peatland. For example, the peat dome at our primary site currently has a mean peat depth of 3.88 m (max 4.92 m) and stores about 1,535 metric tons (t) $C \cdot ha^{-1}$; however, if the climate remains similar to the climate during its

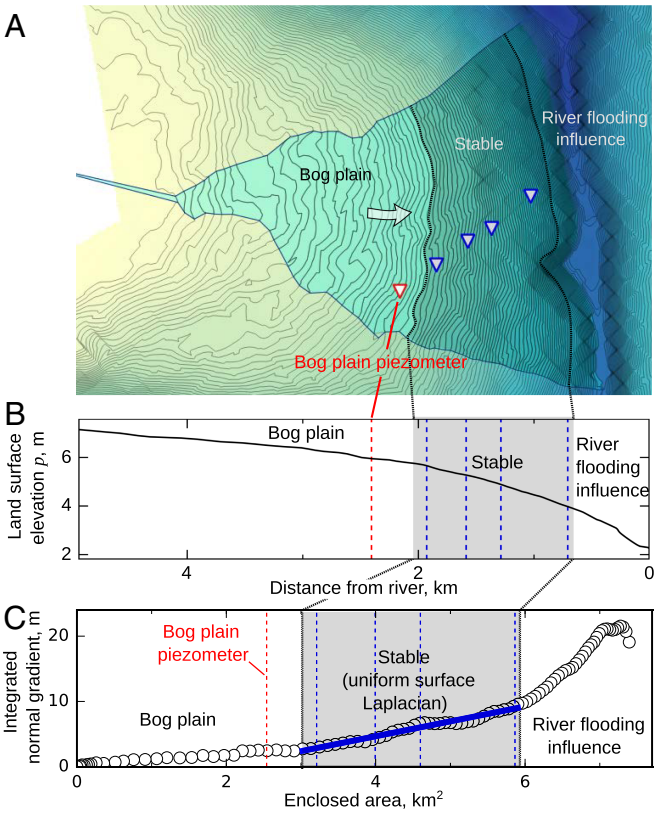

Fig. 6. Estimation of peat surface Laplacian. (*A*) Regions of different morphology and water table behavior within the flow tube used for field site simulations and locations of piezometers (triangles). Farthest from the river, the land surface is relatively flat (bog plain), next there is a region in which the Laplacian of the land surface elevation is uniform ("stable"), and finally there is a narrow region near the river where hydrologic processes and peat accumulation are affected by the rise and fall of the bounding river ("river flooding influence"). (*B*) Profile of LiDAR land surface elevation from *A*, showing piezometer locations (vertical dashed lines). (*C*) Normal gradient driving efflux, integrated along contours, vs. enclosed area. The slope in the stable region gives the average land surface Laplacian of the land surface there and was used for calibration of hydrologic parameters.

2,300-y development, we predict that in about 2,500 y it will reach a stable shape with a mean peat depth of 4.54 m (max 7.10 m) and store 1,800 t C · ha^{-1} (Fig. S3; simulations of dynamics are described in the next section).

The uniformity of the stable peat surface Laplacian is an approximation that requires that (*i*) peat accumulation rate $\partial p/\partial t$ is a nondecreasing function of water table height, (*ii*) flow of water is proportional to water table gradient (Boussinesq's equation), and (*iii*) transmissivity is independent of location because flow through deep peat is negligible compared with near-surface flow. In reality, groundwater flow through deeper peat will result in a deviation of the stable peat dome surface from the uniform-Laplacian shape in very large peat domes. Specifically, groundwater flow through deep, low-permeability peat will tend to flatten the dome center, because of slow infiltration of water into the deep peat, and steepen the dome margin, because of exfiltration of water back into the high-permeability near-surface peat near the boundary. Deep groundwater flow should be manifested as a downward (dome center) or upward (dome margin) trend in the water table during nights without rain when the water table is low; no such trend is apparent in our piezometer data (Fig. 5*D*), suggesting that deep groundwater flow is small. A small deep groundwater flow term is further supported by radiocarbon dating of porewater dissolved organic carbon at our site (31), which suggests a maximum downward velocity of water of about 1 m/y or at most a 1.4-mm water table decline during a single 12-h night, 1/16th of the 22-mm water table decline from evapotranspiration during the day (Fig. 5). (Evapotranspirative flux is about 1/10th of the rate of decline of the water table from evapotranspiration because about 1/10th of the deep peat cross-section is available for water flow; see specific yield curve in Fig. 5*B*.)

A shape parameter related to our stable peatland Laplacian (Eq. **7**) appeared in Ingram's model for temperate peatland morphology (10) assuming constant precipitation, uniform hydraulic conductivity, and simple river geometry (Ingram's parameter is net precipitation divided by hydraulic conductivity, instead of average transmissivity). Our result is more general, because it handles varying rainfall and arbitrary landscapes, but is also mathematically simpler, because of our finding that transmissivity in tropical peatlands is approximately independent of peat depth.

Dynamics of Tropical Peatland Topography and Carbon Fluxes.

Peat accumulation parameters regulate dome dynamics. Our analysis shows how the rate of peat production f_p and decomposition rate constant α affect both the stable morphology and the dynamics of tropical peat domes. These parameters of the peat accumulation function (Eq. **2**) have an indirect but strong effect on the stable peat surface Laplacian and hence peatland carbon storage capacity via the mean transmissivity $\langle T \rangle$ (Eq. **7**) because the mean water table depth must be equal to the ratio of the peat production rate to the decomposition rate constant (f_p/α; Eq. **3**). A higher decomposition rate constant implies a higher mean water table in stable peat domes, meaning

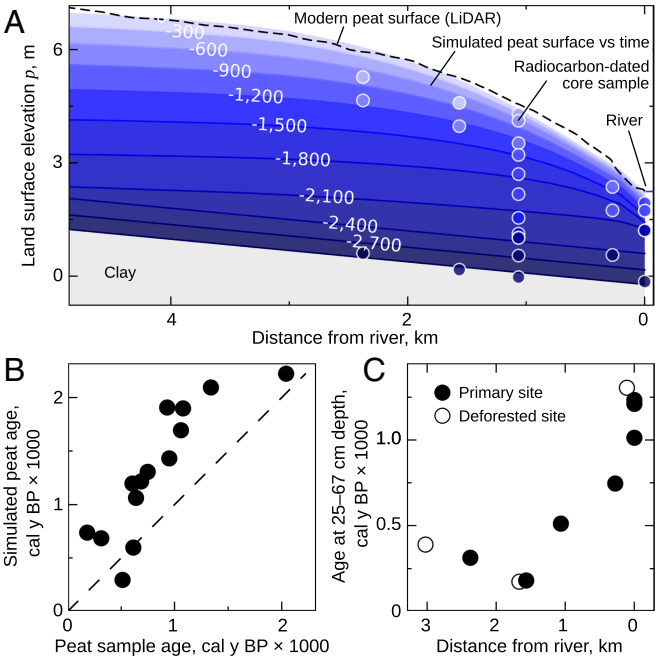

Fig. 7. Morphogenesis of Mendaram peat dome. (*A*) Shape of peat dome over time, including modeled peat surface (contours), modern peat surface from LiDAR (dashed black line), and calibrated radiocarbon dates from peat core samples (colored circles). The deepest peat layers before 2,250 cal y BP represent a uniformly deposited mangrove peat on a gently sloping clay plain (27). (*B*) Simulated age of peat vs. calibrated radiocarbon ages from samples in the Mendaram peat dome. (*C*) Age of shallow peat samples (25–65 cm depth) vs. distance from river at a primary site (solid circles) and a nearby deforested site (open circles). Note the old peat near the surface close to the river as predicted by the model.

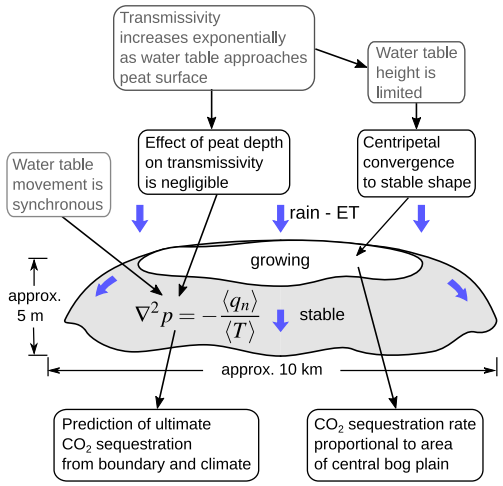

Fig. 8. Model of tropical peat dome development. The surface p of a tropical peat dome evolves toward a shape completely described by a uniform surface Laplacian $\nabla^2 p_\infty$ given by the ratio of average net precipitation $\langle q_n \rangle$ to average hydraulic transmissivity $\langle T \rangle$. The surface Laplacian $\nabla^2 p_\infty$ defines the stable shape and carbon storage capacity of a peat dome inside any drainage boundary. When the dome surface has a uniform Laplacian, the water table height fluctuates uniformly, and peat production is balanced by decomposition everywhere in the dome. When a peat dome is growing, it sequesters carbon at a rate proportional to the area of a flatter (smaller-magnitude surface Laplacian) area in the middle, the central bog plain. Gray boxes, established results; black boxes, findings presented here.

a higher transmissivity, a smaller stable surface Laplacian, and less carbon storage. If both peat production f_p and the decomposition rate constant α increase together, carbon storage capacity does not change, but peat dome dynamics are faster.

Fit parameters match literature data. Peat accumulation parameters fitted to the topography of a peat dome at our Brunei field site agree with published data from other sites and also with our other field data (next section). We obtained peat accumulation parameters f_p, α by simulating the evolution of the dome (Fig. 7) and minimizing the least-squares difference between the simulated peat surface and the modern peat surface measured by LiDAR. We then compared our calibrated peat accumulation function to literature data on subsidence in drained, vegetated peat swamps (4, 22). Our linear peat accumulation function was not calibrated to these subsidence data from the literature—only to the modern peat surface—but nonetheless matched the subsidence data almost exactly (Fig. 4*A*; $f_p = 1.46$ mm $\cdot$ y^{-1}, $\alpha = 1.80$ d^{-1}). Our soil CO_2 chamber measurements were also very similar to those from other sites, suggesting that the effect of water table on fluxes is similar at our site and in other tropical peatlands (Fig. 4*B*).

The uniform-Laplacian principle predicts a central bog plain and old peat near the surface at bog margins. We find that a tropical peat dome reaches its stable shape first at its boundaries, because the stable dome surface is lowest there (Figs. 7 and 8 and Fig. S2). Meanwhile, the interior of the peat dome continues growing at an approximately uniform rate, forming a relatively flat (smaller-magnitude Laplacian) central bog plain. The vegetation of tropical bog plains may not be distinct (1), unlike the unforested bog plains of high-latitude peatlands (21); instead, we define the bog plain of a tropical peat dome as the central region that has not yet reached its stable Laplacian. Whereas the dome center continues to accumulate peat and sequester carbon, the margin has reached its stable shape and stopped growing, so peat near the surface is older there.

Older peat near dome margins has not been predicted before, so we collected 22 additional radiocarbon dates from basal and near-surface peat samples to test this prediction. These radiocarbon dates confirmed that near-surface peat was older near dome margins than at the same depths toward the interior of the same domes (Fig. 7*C*). We also compared radiocarbon dates in deeper peat to simulated ages at the same locations and depths, excluding basal samples from the mangrove peat before the establishment of the peat swamp forest (Fig. 7 and *SI Methods*) (1, 27). Radiocarbon dates and simulated ages at the same locations and depths matched well (Fig. 7*B*). We did not expect radiocarbon dates from cores to match simulated peat ages exactly because (*i*) the drainage network may have shifted during the 2,300 y of dome growth, (*ii*) tree root growth may inject young carbon into peat below the surface, and (*iii*) tree falls in peat swamp forests remove older peat to form tip-up pools that then fill with younger peat. In an earlier study, we estimated that replacement of older peat by younger peat in tip-up pools would bias radiocarbon dates of deep peat to about 500 y later than when material was first deposited in that stratum (figure 11 in ref. 27), consistent with the offset between measured radiocarbon dates and ages simulated by our model (Fig. 7*B*).

Carbon sequestration rate is proportional to bog plain area. The centripetal pattern of dome development makes the rate of carbon sequestration roughly proportional to the area of the central

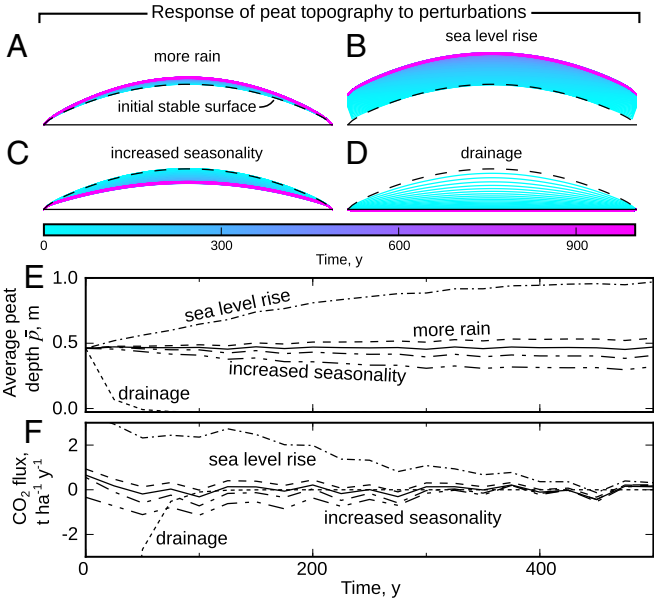

Fig. 9. Dynamic effects of climate change on carbon storage in tropical peatlands. (*A–D*) Simulated peat surface elevation vs. time of an initially stable peat dome after different perturbations. The dashed line indicates the stable morphology for the peat dome between two parallel rivers, and colored lines give the peat dome morphology at subsequent time steps. (*A*) Annual rainfall increase from 2,237 mm/y to 2,430 mm/y causes peat accumulation until the peat dome reaches a new stable morphology. (*B*) Sea level rise of 0.5 m leads to an upward shift in peat surface elevation as tidal rivers bounding the peat dome rise. (*C*) Increase in seasonal fluctuation in rainfall from 902 mm/y to 1,095 mm/y causes loss of peat. (*D*) Sustained drainage to a depth of 50 cm drives rapid peat loss from aerobic decomposition. (*E*) Spatially averaged peat depth vs. time for simulations with more rain (*A*, long-dashed line), sea level rise (*B*, dotted-dashed line), increased seasonality (*C*, dotted-dotted-dashed line), drainage (*D*, short-dashed line), or no change in conditions (solid line) or increased ENSO signal (long dotted-dashed line). (*F*) Average CO_2 emission (negative) or sequestration (positive) vs. time for simulations as in *E*. Because peat is mostly organic carbon, peat accumulation or loss causes uptake or release of carbon, respectively. The initial CO_2 emission for the drainage scenario is off the chart at -24 t $\cdot$ ha^{-1} $\cdot$ y^{-1}.

bog plain (Fig. 8). Under a given climate, the rate of sequestration decreases as the dome approaches its stable shape and the central region of peat accumulation—the bog plain—shrinks in area. For example, our simulations imply that the current rate of CO_2 sequestration at our site (0.80 $t \cdot ha^{-1} \cdot y^{-1}$, 100-y average) is less than one-quarter of its initial rate about 2,300 y ago (3.81 $t \cdot ha^{-1} \cdot y^{-1}$), and CO_2 sequestration is more than five times faster at the dome interior (1.89 $t \cdot ha^{-1} \cdot y^{-1}$, 6.37 km from the river) than at its edge (0.36 $t \cdot ha^{-1} \cdot y^{-1}$, 1 km from the river; Fig. S3). The mechanism of tropical peat dome development that we describe therefore creates landscape-scale patterns in local carbon fluxes and radiocarbon date profiles. Local measurements of carbon fluxes or radiocarbon dates cannot be upscaled to regional fluxes without considering dome morphology because the flatter interior of each peat dome sequesters carbon whereas the margins do not (Fig. 8). Old peat near the peatland surface (2), although in some cases caused by local climate change or disturbance, also can be expected at the margin of any peat dome.

Future Effects of Changes in Drainage Networks and Climate. Our analysis provides a simple way of predicting long-term change in peat dome morphology and carbon storage in response to changes in drainage network, climate, or sea level because the stable peat surface Laplacian completely specifies the stable peat topography with given drainage boundary conditions. If the drainage network changes, we can solve Poisson's equation in the new drainage boundary to compute the gain or loss of peat, and the net carbon emissions, as the peat surface approaches its new stable topography. If the climate changes, we can compute a new stable Laplacian value for the new climatic conditions and determine how much a currently stable peatland will grow or subside.

Subdivision of a peatland by drainage canals reduces carbon storage. The average surface elevation of a stable peat dome is proportional to the area of the dome because of the uniform-Laplacian principle. If we scale the area of a peat dome by some factor k by multiplying both x and y coordinates by $\sqrt{k}$, the surface elevation p must increase by the same factor k to keep the same Laplacian. Therefore, the carbon storage capacity of a peat dome scales with its area. For example, a peat dome that is cut into halves of approximately the same shape as the original dome will have one-half the carbon storage capacity (half the mean stable peat depth) of the original dome. This provides a straightforward way to estimate the long-term impacts of artificial drainage networks that are now affecting over 50% of the peatlands of Southeast Asia (32) and from which a robust quantification of carbon emissions is urgently needed (6).

The dynamic response of a peat dome to changes in rainfall and sea level also depends on its area because of the centripetal pattern of dome development (Fig. 8). Because of their higher stable mean depth, larger-area domes reach their stable shape more slowly than smaller-area domes.

Relative effects of climate change on carbon storage capacity are independent of drainage network. Although peatland drainage networks play a central role in determining absolute carbon storage and dynamics, we can calculate the proportional effect of climate change on long-term carbon storage of a tropical peatland independent of the drainage network. Poisson's equation (Eq. **7**) must be solved in each drainage boundary to obtain the topography of the stable peat surface. However, we can then predict the effects of changes in climate independent of the drainage network because of the linearity of the Laplacian operator. By the definition of linearity for a mathematical operator, a peat surface Laplacian that is larger by some factor k corresponds to a peat surface that is vertically stretched by the same factor ($k\nabla^2 p = \nabla^2 kp$) and therefore has a mean peat depth that is larger by the same factor. Thus, carbon storage capacity per area $\bar{p}_\infty$ is proportional to the stable peat surface Laplacian $\bar{p}_\infty \propto \nabla^2 p_\infty$.

Dynamic simulations converge to new stable morphologies after changes in conditions. Our simulations of peat dome dynamics demonstrate the convergence of initially stable domes to new, stable, uniform-Laplacian morphologies after perturbations (Fig. 9). The simulations show the effect of increased total rainfall (Fig. 9 *A* and *E*), which is a recognized climate feedback for tropical peatlands (12), and also show that artificial drainage for agriculture (Fig. 9*D*) can dominate all natural feedbacks if not curtailed (4, 16). In addition, our simulations demonstrate a third feedback: The increase in rainfall variability from warming climates (33) can cause peat loss if not compensated by an increase in total rainfall (Fig. 9 *C* and *F*). For these simulations, we generated new rainfall time series as similar to current rainfall as possible but with larger annual and El Niño–Southern Oscillation (ENSO) fluctuations (Fig. S4 *A* and *B* and *SI Setting Annual and ENSO Amplitudes of Rainfall*). Either greater seasonality or a stronger ENSO decreased peatland carbon storage capacity, but an increase in seasonality had a larger maximum effect, partly because the magnitude of the ENSO fluctuation is smaller. In contrast, sea level rise could drive peat accumulation in the long term by elevating the tidal rivers draining most peat domes (Fig. 9 *B* and *E*). In general, losses can be much more rapid than accumulation (Fig. 9*E*), because subsidence of drained peatlands can be far faster than typical accumulation rates (4). For example, the estimated area-averaged current CO_2 sequestration rate at our site is 0.80 $t \cdot ha^{-1} \cdot y^{-1}$, whereas Hooijer et al. (5) estimated CO_2 emissions of at least 73 $t \cdot ha^{-1} \cdot y^{-1}$ from tropical peatlands under plantation agriculture.

Intermittency of rainfall reduces tropical peatland carbon storage. We find that fluctuations in net precipitation on timescales from hours to years can reduce long-term peat accumulation. We further explored the effects of variability in rainfall seen in our

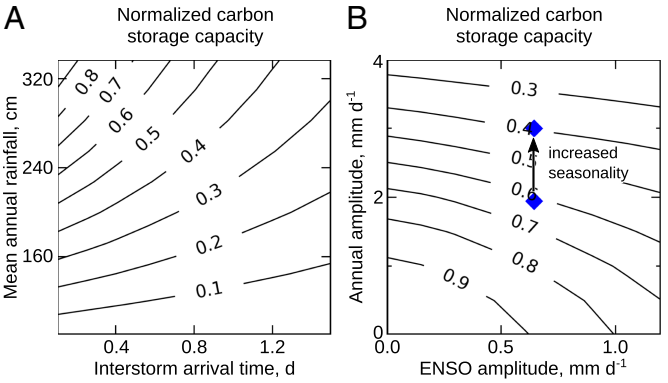

Fig. 10. Effects of climate change on carbon storage capacity of tropical peatlands. (*A*) Simulated carbon storage capacity (contours) vs. time-averaged rainfall and interval between storms in a simple rainfall model (Poisson process for storm incidents, exponentially distributed rain depth per storm). The balance between rainfall and groundwater flow sets a limit on the curvature of the peat surface and therefore limits the amount of carbon that can be stored as peat in a peatland. This carbon storage capacity is proportional to the Laplacian of the stable peat surface elevation (*Results and Discussion*), so the relative effect of changes in rainfall patterns on carbon storage capacity can be calculated independent of the drainage network. Higher rainfall increases carbon storage capacity, whereas increased time between storms reduces it. (*B*) Carbon storage capacity (contours) as in *A*, but driven by rainfall at our site (diamond) or with a weakened or strengthened annual or El Niño–Southern Oscillation fluctuation in rainfall. The vertical shift to lower carbon storage with increased annual variation in rainfall (up arrow) corresponds to the simulated effect of increased seasonality in Fig. 9.

dynamic simulations (Fig. 9) by computing the effect of interstorm arrival time and annual and ENSO fluctuations on peatland carbon storage capacity (Fig. 10). The simulations demonstrate that long-term peat accumulation is controlled by variation in rainfall, not only by mean rainfall, because fluctuations in the water table cause exponential changes in groundwater flow. The high outward flow during peak water tables is not compensated by low flow rates after the water table declines. For example, a steady drizzle at the same average intensity as the intermittent rainfall actually observed at our site would sustain more than 10 times more long-term carbon storage (19.5 $kt \cdot ha^{-1}$ vs. 1.80 $kt \cdot ha^{-1}$; Fig. S4 *D* and *E*). The intermittency of tropical convective storms significantly affects long-term carbon storage: Carbon storage capacity can decrease by one-third depending on whether convective storms arrive every 14 h on average, as at our site, or every 24 h, with the same mean rainfall (Fig. 10*A*).

Our simulations with smoothed rainfall intensity and evapotranspiration show that models must consider the effects of subdiurnal fluctuations in rainfall to correctly predict the long-term evolution and carbon storage of tropical peatlands. The exact details of the fluctuations in rainfall are not important, in the sense that many distinct rainfall time series can give the same stable surface Laplacian and the same carbon storage capacity. However, carbon storage capacity can be severely overestimated by simulations that entirely ignore the effects of fluctuations in rainfall. We explored the effects of neglecting fluctuations in rainfall by computing the stable surface Laplacian after averaging net precipitation on hourly and longer intervals. Treating rainfall intensity and evapotranspiration as constant each hour, instead of every 20 min, increased the simulated stable surface Laplacian by a few percent, but averaging over 1 d led to an overestimate by 20%, over 1 wk by 100%, over 1 mo by 400%, and over 1 y by more than 1,000% (Fig. S4 *D* and *E*).

Conclusions

The mathematical and numerical models presented here predict the long-term effects of changes in rainfall regimes and drainage networks on the morphology of tropical peat domes. Because tropical peat domes are mostly organic carbon, these predictions of peat dome morphogenesis also quantify peat dome carbon storage capacity and carbon fluxes. Our approach shows that tropical peatlands approach a limiting shape in which the Laplacian of the land surface is uniform. This stable peatland surface Laplacian can be computed from any rainfall time series and completely summarizes the effects of the rainfall pattern on the stable morphology and storage capacity of carbon within the peatland drainage boundary.

The uniform-Laplacian principle is supported by a range of observations: (*i*) The peat surface Laplacian is approximately uniform in a region near the dome edge (Fig. 6*C*); (*ii*) water table behavior is uniform where the surface Laplacian is uniform and is different in the dome interior (Fig. 5*A*); (*iii*) water table behavior is the same in areas with differing gradients within the uniform-Laplacian region (Fig. 5*A*); (*iv*) transmissivity increases exponentially at high water tables, so that local water balance is dominated by flow near the surface (Fig. 5*C*); and (*v*) peat accumulation parameters match literature data, even though those data were not used for calibration (Fig. 4*A*).

Our analysis underscores the importance of considering geomorphology when measuring and modeling carbon fluxes in tropical peatlands. On a growing peat dome, the perimeter of the dome reaches a steady elevation first while central areas continue to accumulate carbon (Fig. 8). This pattern of dome morphogenesis implies that the locations of ground-truth carbon flux measurements within tropical peat domes are important considerations for earth system models (34). For example, measurements of carbon flux in the center of a growing dome overestimate the average flux for the whole dome, because peat accumulation is fastest in the center (Fig. 8 and Fig. S3). The distribution of peat dome areas within a peatland complex is also important, because smaller domes reach their stable shapes faster after a change in conditions. Improved earth system models could use the uniform-Laplacian principle to efficiently account for the effects of changing rainfall, sea level, and drainage on tropical peat carbon storage, given a realistic distribution of peat dome sizes. The approach outlined here also provides a framework for including the effects of other long-term processes that remain understudied, such as shifts in river networks, changes in tree community composition, and saltwater intrusion from rising sea levels.

ACKNOWLEDGMENTS. We thank Mahmud Yussof of Brunei Darussalam Heart of Borneo Center and the Brunei Darussalam Ministry of Industry and Primary Resources for their support of this project; Hajah Jamilah Jalil and Joffre Ali Ahmad of the Brunei Darussalam Forestry Department for facilitation of field work and release of staff; Amy Chua for logistical support; and Bernard Jun Long Ng, Rahayu Sukmaria binti Haji Sukri, Watu bin Awok, Azlan Pandai, Rosaidi Mureh, Muhammad Wafiuddin Zainal Ariffin, and Sylvain Ferrant for field assistance. We also thank Paul Glaser and two anonymous reviewers for their detailed comments on the manuscript. This research was supported by the National Research Foundation Singapore through the Singapore–MIT Alliance for Research and Technology's Center for Environmental Sensing and Modeling interdisciplinary research program, by the US National Science Foundation under Grants 1114155 and 1114161 (to C.F.H.), and by a grant from the Environmental Solutions Initiative at Massachusetts Institute of Technology.

1. Anderson JAR (1964) The structure and development of the peat swamps of Sarawak and Brunei. *J Trop Geogr* 18:7–16.
2. Dommain R, Couwenberg J, Joosten H (2011) Development and carbon sequestration of tropical peat domes in South-east Asia: Links to post-glacial sea-level changes and Holocene climate variability. *Quat Sci Rev* 30:999–1010.
3. Page SE, et al. (2002) The amount of carbon released from peat and forest fires in Indonesia during 1997. *Nature* 420:61–65.
4. Couwenberg J, Dommain R, Joosten H (2010) Greenhouse gas fluxes from tropical peatlands in Southeast Asia. *Glob Change Biol* 16:1715–1732.
5. Hooijer A, et al. (2012) Subsidence and carbon loss in drained tropical peatlands. *Biogeosciences* 9:1053–1071.
6. Calle L, et al. (2016) Regional carbon fluxes from land use and land cover change in Asia, 1980–2009. *Environ Res Lett* 074011:1–12.
7. Page S, Hooijer A (2016) In the line of fire: The peatlands of Southeast Asia. *Philos Trans R Soc Lond B Biol Sci* 371:20150176.
8. Winston RB (1994) Models of the geomorphology, hydrology, and development of domed peat bodies. *Geol Soc Am Bull* 106:1594–1604.
9. Hirano T, Jauhiainen J, Inoue T, Takahashi H (2009) Controls on the carbon balance of tropical peatlands. *Ecosystems* 12:873–887.
10. Ingram HAP (1982) Size and shape in raised mire ecosystems - A geophysical model. *Nature* 297:300–303.
11. Glaser PH, Hansen BCS, Siegel DI, Reeve AS, Morin PJ (2004) Rates, pathways and drivers for peatland development in the Hudson Bay Lowlands, northern Ontario, Canada. *J Ecol* 92:1036–1053.
12. Lottes AL, Ziegler AM (1994) World peat occurrence and the seasonality of climate and vegetation. *Palaeogeogr Palaeoclimatol Palaeoecol* 106:23–37.
13. Gastaldo RA (2010) Peat or no peat: Why do the Rajang and Mahakam deltas differ? *Int J Coal Geol* 83:162–172.
14. Clymo RS (1984) The limits to peat bog growth. *Philos Trans R Soc Lond B Biol Sci* 303:605–654.
15. Hilbert D, Roulet N, Moore T (2000) Modelling and analysis of peatlands as dynamical systems. *J Ecol* 88:230–242.
16. Kurnianto S, et al. (2015) Carbon accumulation of tropical peatlands over millennia: A modeling approach. *Glob Change Biol* 21:431–444.
17. Morris PJ, Baird AJ, Belyea LR (2012) The DigiBog peatland development model 2: Ecohydrological simulations in 2D. *Ecohydrology* 5:256–268.
18. Baird AJ, Morris PJ, Belyea LR (2012) The DigiBog peatland development model 1: Rationale, conceptual model, and hydrological basis. *Ecohydrology* 5:242–255.
19. Jauhiainen J, Takahashi H, Heikkinen JEP, Martikainen PJ, Vasanders H (2005) Carbon fluxes from a tropical peat swamp forest floor. *Glob Change Biol* 11:1788–1797.
20. Lampela M, et al. (2016) Ground surface microtopography and vegetation patterns in a tropical peat swamp forest. *Catena* 139:127–136.
21. Glaser PH, Janssens JA (1986) Raised bogs in eastern north America: Transitions in landforms and gross stratigraphy. *Can J Bot* 64:395–415.
22. Carlson KM, Goodman LK, May-Tobin CC (2015) Modeling relationships between water table depth and peat soil carbon loss in Southeast Asian plantations. *Environ Res Lett* 10:074006.

23. Melling L, Hatano R, Goh KJ (2005) Soil CO_2 flux from three ecosystems in tropical peatland of Sarawak, Malaysia. *Tellus* 57B:1–11.
24. Ali M, Taylor D, Inubushi K (2006) Effects of environmental variations on CO_2 efflux from a tropical peatland in eastern Sumatra. *Wetlands* 26:612–618.
25. Jauhiainen J, Hooijer A, Page SE (2012) Carbon dioxide emissions from an *Acacia* plantation on peatland in Sumatra, Indonesia. *Biogeosciences* 9:617–630.
26. Hirano T, et al. (2012) Effects of disturbances on the carbon balance of tropical peat swamp forests. *Glob Change Biol* 18:3410–3422.
27. Dommain R, et al. (2015) Forest dynamics and tip-up pools drive pulses of high carbon accumulation rates in a tropical peat dome in Borneo (Southeast Asia). *J Geophys Res Biogeosci* 120:617–640.
28. Hooijer A (2005) Hydrology of tropical wetland forests: Recent research results from Sarawak peatswamps. *Forests, Water and People in the Humid Tropics*, eds Bonell M, Bruijnzeel LA (Cambridge Univ Press, Cambridge, UK), pp 447–461.
29. Dolan TJ, Hermann AJ, Bayley SE, Zoltek J, Jr (1984) Evapotranspiration of a Florida, U.S.A., freshwater wetland. *J Hydrol* 74:355–371.
30. Baird AJ, et al. (2017) High permeability explains the vulnerability of the carbon store in drained tropical peatlands. *Geophys Res Lett* 44:1333–1339.
31. Gandois L, et al. (2014) Origin, composition, and transformation of dissolved organic matter in tropical peatlands. *Geochim Cosmochim Acta* 137:35–47.
32. Miettinen J, Shi C, Liew SC (2016) Land cover distribution in the peatlands of Peninsular Malaysia, Sumatra and Borneo in 2015 with changes since 1990. *Glob Ecol Conserv* 6:67–78.
33. Huang P, Xie SP, Hu K, Huang G, Huang R (2013) Patterns of the seasonal response of tropical rainfall to global warming. *Nat Geosci* 6:357–361.
34. Quéré CL, et al. (2009) Trends in the sources and sinks of carbon dioxide. *Nat Geosci* 2:831–836.
35. Moore ID, Grayson RB (1991) Terrain-based catchment partitioning and runoff prediction using vector elevation data. *Water Resour Res* 27:1177–1191.
36. Stuiver M, Reimer PJ (1993) Extended ^{14}C data base and revised CALIB 3.0 ^{14}C age calibration program. *Radiocarbon* 35:215–230.
37. Reimer PJ, et al. (2013) IntCal13 and MARINE13 radiocarbon age calibration curves 0–50000 years cal BP. *Radiocarbon* 55:1869–1887.
38. Ferziger JH, Perić M (1999) *Computational Methods for Fluid Dynamics* (Springer, Berlin), 2nd Ed.
39. Patankar SV (1980) *Numerical Heat Transfer and Fluid Flow* (Taylor & Francis, Boca Raton, FL).
40. Moerman JW, et al. (2013) Diurnal to interannual rainfall $\delta^{18}O$ variations in northern Borneo driven by regional hydrology. *Earth Planet Sci Lett* 369–370:108–119.
41. Partin JW, Cobb KM, Adkins JF, Clark B, Fernandez DP (2007) Millennial-scale trends in west Pacific warm pool hydrology since the Last Glacial Maximum. *Nature* 449:25–30.
42. Moore JC, Grinsted A, Zwinger T, Jevrejeva S (2013) Semiempirical and process-based global sea level projections. *Rev Geophys* 51:484–522.
43. Roundtable on Sustainable Palm Oil (2013) Principles and criteria for the production of sustainable palm oil. Available at www.rspo.org/key-documents/certification/rspo-principles-and-criteria#.